The Sensitivity of Bridge Safety to Spatial Correlation of Load and Resistance

Donya Hajializadeh[1], Eugene J. OBrien[1,2], Mark G. Stewart[3]

[1] Roughan & O'Donovan Innovative Solutions, Ireland

[2] University College Dublin, Ireland

[3] The University of Newcastle, Australia

Abstract

Random Field theory has emerged in recent years to model the statistical correlation of resistance in concrete structures and to determine its influence on the probability of structural failure. A major shortcoming in the work carried out to date is the spatial variability and corresponding correlation associated with applied traffic loads. In this paper the influence of spatial correlation of both traffic load and resistance is considered in the context of bridge safety assessment. The current study, explores, the nature of the problem by three theoretical examples. As a general trend, examples show that while traffic loads are weakly correlated, load effects are strongly correlated as the same heavy vehicle often causes extremes of load effect in different parts of the bridge which is due to the transverse sharing of load (measured here using a load sharing factor).

It is found that the strength of correlation of load effect depends greatly on the load sharing factor which is treated in a simple way in many studies. In a more sophisticated beam-and-slab bridge example, load sharing factors are derived from a finite element analysis to assess transverse load sharing, and are shown to vary by girder number, girder segment and by load location. Despite the fact that load effect at points along the length of a bridge are strongly correlated, the combined influence of correlation in load and resistance on probability of failure is small

Keywords: random field, spatial, variability, correlation, autocorrelation, traffic, load, WIM

1 Introduction

An accurate assessment of the remaining service life of a structure requires information about the structure and its load and a simulation model which is able to incorporate this information into a safety analysis. The simulation should account for various sources of uncertainty in modelling such as time-dependent variation of structural performance, randomness in loading, and variability of material and geometrical properties. This requires the use of probabilistic methods in a structural safety analysis. Two types of uncertainty, namely the aleatory and the epistemic, are necessary for an accurate probabilistic analysis (Ang and Tang 2007). Whereas randomness (or aleatory uncertainty) cannot be reduced, improvement in knowledge or in the accuracy of predictive models will reduce the epistemic uncertainty (Ang and De Leon 2005). Probabilistic reliability analysis permits the inclusion of these uncertainties into a safety analysis.

In recent times, probabilistic and reliability-based approaches have been widely used to quantify bridge safety (Mori and Ellingwood 1993; Stewart and Rosowsky 1998; Enright and Frangopol 1999; Val et al. 2000; Vu and Stewart 2000; Stewart et al. 2001; Akgül and Frangopol 2004; Stewart et al.

2004; Ellingwood 2005; Stewart and Mullard 2007; Frangopol 2011). While the focus of much of this work has been on the probabilistic description of homogeneous properties, less effort has been directed towards the modelling of the spatial correlations of load and resistance. It is well established that the material properties of a structure and structural dimensions are spatially variable, associated with workmanship and environmental conditions. This results in spatially distributed damage mechanisms such as corrosion-induced cover cracking and spalling. Traffic load and particularly the stresses due to the load, are also spatially correlated.

Allowing for spatial correlation in probabilistic calculation is achieved by Random Field (RF) Theory, and the terms RF and Spatial Variability are used synonymously in the literature. In the RF analysis, the random field is discretised into large numbers of spatially correlated discrete random variables. The structural member is divided into small segments and spatial variation within a segment is neglected. It is implicit that deterioration at a point increases the probability of deterioration at adjacent points. Recent work has demonstrated the advantage of incorporating spatial variability into stochastic models to predict the likelihood and extent of corrosion damage in reinforced concrete (RC) structures (Stewart 2005; Stewart and Mullard 2007; Kenshel and O'Connor 2009; Stewart and Suo 2009).

Engelund and Sørensen (1998) consider spatial variation of the variables associated with the critical threshold for initiation of corrosion of reinforcement, i.e., the coefficient of diffusion of chloride and surface chloride concentration. They estimate the distribution of the time to initiation of corrosion using the First Order Reliability Method (FORM) and Second Order Reliability Method (SORM) analyses. Stewart (2004) considers the spatial variability of pitting corrosion in RC beams. RC beams are discretised into series of segments in one-dimension (1D) random fields and maximum pit depths are generated for each reinforcing steel bar in each element.

Malioka and Faber (2004) suggest that corrosion initiation and propagation are spatially variable due to the general trend seen within concrete batches and workmanship during construction of RC structures. The authors then present a random field approach to model the spatial variability of concrete permeability and use this within a reliability analysis to predict the percentage of a structure that will exhibit degradation at a specified point in time.

Spatial variability research carried out to date has been mainly focused on predicting the performance of corroding structures and spatial variability of the common parameters such as material, dimension and environmental properties (Li et al. 2004; Karimi et al. 2005; Stewart 2005; Vu and Stewart 2005; Darmawan and Stewart 2007; Marsh and Frangopol 2008; Kenshel and O'Connor 2009; Akiyama et al. 2010; Zhai and Stewart 2010). A major shortcoming in the work to date is that the spatial variability and corresponding correlation associated with applied loads and load effects has not been allowed for.

Analysis of measured traffic data shows there are patterns of correlation and interdependence between vehicle weights, speeds and inter-vehicle gaps , both within lanes and between adjacent lanes in same-direction traffic (OBrien and Enright 2011). Correlation between weights of successive vehicles can arise from a number of causes. There are times of the day at which heavy vehicles are more likely to travel, and these intra-day patterns are one reason why there is a weak but non-zero level of correlation between vehicle weights within each lane. Furthermore, heavy vehicles from the same company can sometimes travel together.

In the work by Nowak (1993), a number of simplifying assumptions are made – for instance, that one in 15 heavy trucks has another truck side-by-side, and that for one in 30 of these multiple-truck events, the two trucks have perfectly correlated weights. A heavy truck is defined as one with a Gross Vehicle Weight (GVW) in the top 20% of measured truck weights. It is calculated that the maximum load effect in 75 years is caused by two trucks side-by-side, with each truck having a GVW of 85% of the maximum individual GVW in 75 years. As Kulicki et al. (2007) note, the assumptions used are based on limited observations, and no data is utilised for the assumptions on weight correlation; they are entirely based on judgment.

Sivakumar et al. (2007) refine the definition of side-by-side events to include two trucks with headway separation of ±18.5 m (60 ft), and also consider the influence of the bridge length. Sivakumar et al. (2011), citing Gindy and Nassif (2007), extend this further by classifying multiple-presence events as side-by-side, staggered, and following or multiple. They present statistics, derived from weigh-in-motion (WIM) measurements, for the frequency of occurrence of these events for different truck traffic volumes and bridge spans. They describe a method for estimating site-specific bridge loading which uses multiple-presence probabilities calculated either directly from WIM data or estimated from traffic volumes using reference data collected at other sites. It is assumed that there is no correlation between weights in adjacent lanes and that the GVW distribution is the same in both lanes. The latter assumption, in particular, has been shown to be inconsistent with measurements (OBrien and Enright 2011).

OBrien and Enright (2011) introduce ‘scenario modelling’ as a method of simulating traffic that is relatively simple to apply. It is found that, even though traffic load is very slightly correlated, load effects are strongly correlated and gaps in adjacent lanes are closely linked. The correlated traffic is found to give a better fit to the measured data than models which assume no correlation. A least squares measure is used to quantify the goodness of fit of the two simulation models to the measured load effects. For this purpose, ratios which compare the goodness of fit of simulated daily maximum load effects from the uncorrelated and smoothed bootstrap model are averaged across all relevant load effects and bridge lengths. In this comparison ratios significantly greater than 1 mean that the smoothed bootstrap model gives a better fit. It is found that in most cases the ratio is higher than 1.5(OBrien and Enright 2011).

In this paper, three numerical examples are presented, of varying complexity, to explore the spatial variability of load and load effect and the spatial variability of resistance, and examine the effect of these correlations on the probability of failure. First, a single-span ‘bridge’ consisting of two side-by-side beams is considered (i.e., transverse interaction is ignored). Correlation of resistance and load is examined for a segment at mid-span of the bridge. Single point loads are applied on each beam. In the second example, point loads are again used on a single-span bridge made up of two side-by-side beams. However, in this case, the loads are assumed to travel across the bridge and their relative position is allowed to vary randomly to better simulate actual traffic loading. The effect of considering all segments, rather than just the mid-span, is also investigated. Finally, a more realistic example is considered that illustrates the same concepts identified in the simpler examples. In this final example, a probabilistic load model is applied to a 2D beam and slab (girder) bridge. Like the HL-93 model, there is a moving three-axle truck combined with a uniformly distributed load (UDL). The truck weight and the intensity of the UDL are assumed to be from Weibull distributions with parameters that give an approximate match with measurements collected on 20m bridge in the Netherlands. In other words, these three examples investigate the following unanswered issues: (1) Effect of load correlation on load effect correlation and hence probability of failure; (2) Effect of load sharing factor on load effect correlation and hence probability of failure; (3) The effect of combined

load and resistance correlation on probability of failure; (4) Sensitivity of probability of failure to correlation coefficient of load and resistance and order of magnitude; (5) Effect of considering the possibility of element failure which are not necessarily at the mid-span for a simply supported bridge.

For this study, the authors combine models that allow for the spatial variability of resistance and the spatial variability of load and load effect. The influence of load correlation on probability of failure is investigated and its interaction with correlation of resistance.

2 Nature of Correlation

Correlation Coefficient for load and resistance

In the three examples considered in the current study, the random variables include: (i) loads on each lane, and (ii) resistances for each segment of each lane. For example, in the second example, a two-lane bridge has 14 segments in each lane, and two loads (one each on lanes 1 and 2) giving twenty eight resistances. Each random variable is assigned a probability density function (PDF) $f_{Xi}(x_i)$. In this study, the Pearson coefficient of linear correlation, ρ_{ij}, is used as a measure of the degree of linear dependence between the two variables and is referred to as the "coefficient of correlation" throughout this paper.In the current paper, the traffic load is assumed to be independent of distance and it is correlated using the constant correlation coefficient, ρ_P. In this study, *P* stands for load, *S* for load effect resulting from *P*, and *R* refers to resistance. For resistance, two different correlation terms are included: constant and distance-dependent:

$$\rho_R(\tau) = \rho_{R0} + (1 - \rho_{R0}) exp\left(-\left(\frac{\tau_x}{d_x}\right)^2 - \left(\frac{\tau_y}{d_y}\right)^2\right) \quad (1)$$

where ρ_{R0} represents the constant component of correlation (e.g., workmanship will vary from site to site). The second term relates to inter-segment distances: $d_x = \theta_x / \sqrt{\pi}$; $d_y = \theta_y / \sqrt{\pi}$, where θ_x and θ_y are termed 'scales of fluctuation' and quantify the extent of the spatial correlation in the x and y directions respectively. The terms, $\tau_x = x_{j+1} - x_j$; $\tau_y = y_{j+1} - y_j$ are distances between centres of segments j and $j + 1$ in the x and y directions respectively (Li et al. 2004). Equation (1) is referred to as the autocorrelation function (Vanmarcke 1985; Haldar and Mahadevan 2000; Li et al. 2004; Kenshel and O'Connor 2009). It determines the correlation coefficient between two segments separated by distance τ and is representative of the spatial correlation between the segments. As the distance between correlated segments increases, the correlation coefficient reduces.

To illustrate the effect of the distance-dependent term in Equation (1), Figure 1 shows the one-dimensional form of the function. It can be seen that the distance-dependent term has almost zero effect for segments 4 m apart, i.e., only the immediately adjacent segments are affected by that term.

A number of autocorrelation functions can be formulated, such as triangular, exponential and Gaussian but the validation of these requires large amounts of spatial data that is often not available. The Gaussian (or squared exponential) correlation function (second term in Equation (1)), is commonly used in engineering applications, particularly for spatial modelling of RC structures (Li and Der Kiureghian 1993; Kersner et al. 1998; Haldar and Mahadevan 2000; Vu 2003; Malioka and Faber 2004; Stewart 2006; Sudret et al. 2007).

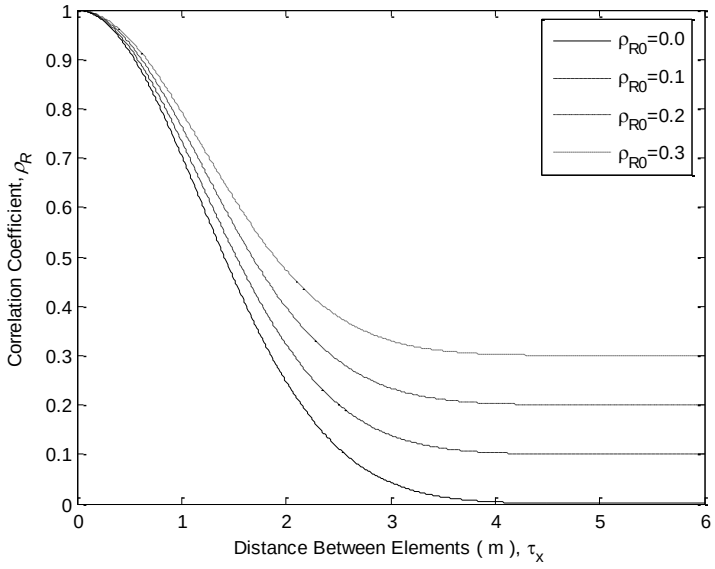

Figure 1 – Resistance correlation coefficient for 1D autocorrelation function

The scale of fluctuation, θ, introduced in Equation (1), defines the distance over which significant correlation persists in a random field. Vanmarcke (1985) proposes various methods for the calculation of the scale of fluctuation for stationary random fields. These methods, however, require large amounts of spatial data and although this has been collected in some cases (Karimi 2002; O'Connor and Kenshel 2012), typically the scale of fluctuation is estimated using engineering judgement. The value of the scale of fluctuation should be chosen in conjunction with an appropriate random field segment size so that mathematical and computational difficulties are avoided.

Segment Size

As discussed, the random field is discretised into a number of segments within which the value of the random field is considered constant and the inter-segment correlation is calculated using the correlation function. The size of the discretised segment is usually defined based on practical and analytical considerations (Sterritt et al. 2001). The use of a fine mesh can significantly increase the computational effort for little improvement in accuracy. Further, a smaller segment size can mean that segments close to each other are highly correlated, resulting in numerical and computational difficulties in the orthogonalisation of the covariance matrix. Conversely, if the segment size is too large, the correlation between segments becomes negligibly small.

Der Kiureghian and Ke (1988) suggest that the size of the segments should be one fourth to one half of the correlation length. Therefore for a scale of fluctuation of 3.0 m, a segment size of 1.5 m is recommended.

Probability of failure

A probability of structural failure can be computed as soon as each segment is assigned a resistance (R) and load effect (S) corresponding to the load which the structure is subjected to. The operating scenario is the availability of a resistance greater than the load effect, i.e., such that $G = R - S > 0$, and the non-operating or failure scenario is $G = R - S \leq 0$; the measure of failure is then the probability associated with the event $[R - S \leq 0]$, that is:

$$\text{Probability of failure} = P_f = Prob([R - S \leq 0]) \quad (2)$$

Theoretically, the solution to Equation (2) can be obtained through one of the following methods: (1) direct analytical integration, (2) numerical integration, such as Monte Carlo simulation or (3) by transforming the integrand into a multi-normal joint PDF for which some results are available. These methods have been described in detail in many classical references (Melchers 1999; Haldar and Mahadevan 2000). Except for some special cases, the integration of Equation (2) over the failure domain $G(X) \leq 0$ cannot be performed analytically (Melchers 1999). The reliability problem which incorporates RF models (i.e., takes into consideration the uncertainty associated with spatial variability) usually results in a large number of random variables. Furthermore, many of the model parameters are statistically and/or physically dependent and their mathematical representations are of a nonlinear nature. Consequently, the $G(X)$ function and the failure domain cannot be easily expressed or approximated by an analytical model (Papadrakakis and Lagaros 2002; Vu et al. 2005).

As the number of random variables increases and the problem becomes more complex, Monte Carlo (MC) simulation-based methods are found to be more reliable (Papadrakakis and Lagaros 2002). In each MC realisation, $G(X)$ is evaluated for each segment of the structure and failure is defined by the violation of $G(X)$ for any segment, i.e., failure is when the minimum of $G(X)$, for all segments, is ≤ 0.

3 Example 1: Two-Point Problem with Stationary Loads

To illustrate the basic concepts of load and resistance correlation, a notional 21 m long simply supported bridge is considered, consisting of just two side-by-side beams, one under each of two lanes, connected by some transverse members (e.g., slab). Each beam is subject to a stationary centrally located point load and only these two points are considered in the analysis (i.e., side-by-side loads at mid-span). Initially the loads are assumed to be uncorrelated and there is no transverse loading sharing. Probabilities are derived assuming the loads to be from a bivariate Normal distribution with means of, $\mu_1 = \mu_2 = 410$ (kN) and standard deviations of $\sigma_1 = \sigma_2 = 41$ (kN) for loads 1 (P_1) and 2 (P_2) respectively. Figure 2 gives contours of the resulting probabilities. It can be seen that the contours are circular as there is no correlation between loads – 'diagonal' and off-diagonal combinations of load are equally frequent (Figure 2).

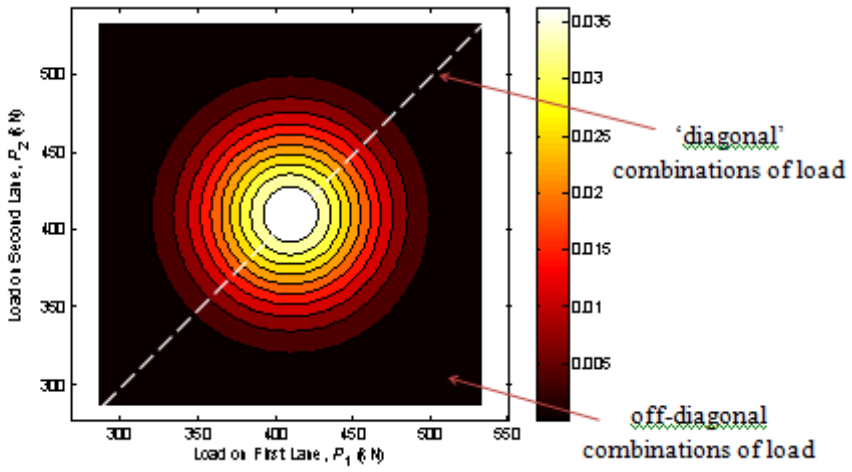

Figure 2 – Contours of probability for load combinations (uncorrelated case)

The mid-span bending moment load effects are calculated for each lane and multiplied by a "load sharing factor", λ, to account for transverse load sharing. The lane for which load effect is calculated is identified as the "primary" lane and the load sharing factor for vehicles in this lane is taken as unity. When a load is also present in the other "secondary" lane, the contribution of the load to load effect in the primary lane is represented by the load sharing factor. The load sharing factors used in this example cover the range of those reported from a finite element study by Enright (2010).

The load sharing factor causes the load effects to be correlated, even when the loads are not – a large load in one lane causes high load effect in both lanes so the probability of both load effects being high is increased. As shown in Figure 3(a), the diagonal terms in a plot of load effect in beam 1 (S_1) against load effect in beam 2 (S_2) are now more frequent than the off-diagonal terms. This correlation between load effects gets stronger as the load sharing factor increases.

When correlation between the two loads is introduced, the probabilities of the diagonal combinations of load increase at the expense of the off-diagonal combinations. As a result the contours of probability become 'more oval' (Figure 3(b) – the major axis length on the outermost oval is increased from 1440 to 1715 and the minor axis is shortened from 498 to 21). It can be concluded that load effect is strongly influenced by load sharing factor which makes it strongly correlated, even when load is not correlated. The correlation of load increases this trend. It should be noted that the magnitude of correlation (i.e., 0.4) is exaggerated in this example and is much higher than what would be expected in reality.

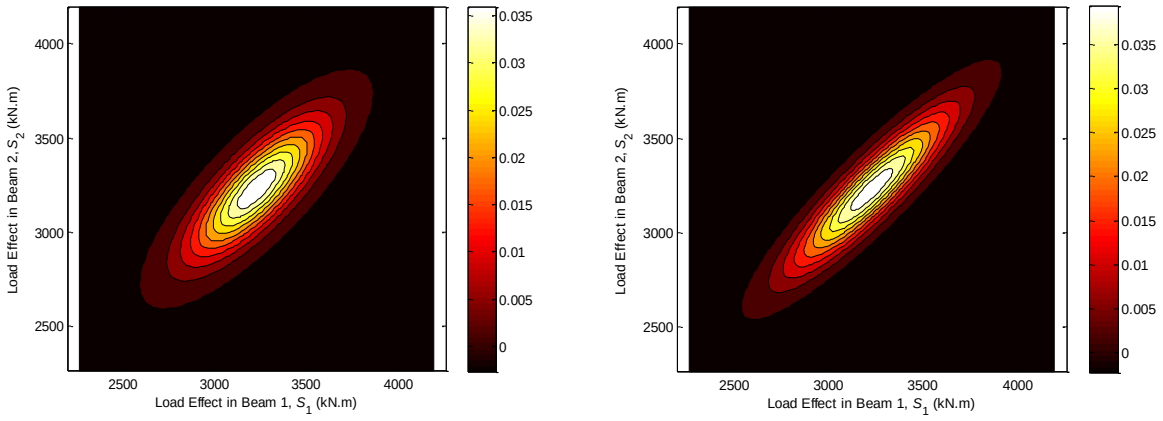

(a) (b)

Figure 3 – Contours of probability for load effect combinations: (a) uncorrelated load; (b) load correlation coefficient of 0.4

The resistances of the two beams are also taken to be from a bivariate Normal distribution, in this case, with means of, $\mu_1 = \mu_2 = 4650$ (kN.m) and standard deviations of, $\sigma_1 = \sigma_2 = 400$ (kN.m) for beams 1 and 2 respectively. Given the resistance and load effect values for mid-span, the probability of failure can be calculated using Equation (2). Failure is said to occur when the load effect at the mid-point of either of the two beams exceeds the resistance. In practice, failure only occurs in extreme load effect cases so only the top right corner of the load effect figures (Figure 3a,b) are of interest. Increasing the correlation of load effect causes an increased probability of *both* load effects being extreme but a reduced probability of *either* load effect being extreme, i.e., the probabilities in the top right increase at the expense of the top middle and right middle. In mathematical terms, the probability of failure is defined as:

$$P_f = P(S_1 > R_1, S_2 \leq R_2) + P(S_1 \leq R_1, S_2 > R_2) + P(S_1 > R_1, S_2 > R_2) \qquad (3)$$

where S_1, S_2 are load effects and R_1, R_2 are resistances. Correlation has the effect of increasing the third term while decreasing the 1st and 2nd. The probability of failure can be expressed more simply in complementary form, as:

$$P_f = 1 - P(S_1 \leq R_1, S_2 \leq R_2) \quad (4)$$

Even for the bivariate Normal distribution, there is no closed form solution for this joint probability of both load effects being less than their respective resistances and it can be increased or decreased by correlation.

Figure 4 shows the effect of different levels of correlation on the probability of failure, assuming the same range of correlation for load (ρ_P) and resistance (ρ_{R0}). The baseline case is when both load and resistance are independent, i.e., no correlation (IL-IR). In Figure 4(a), when load sharing factor is, $\lambda = 0.5$, and when only load is correlated (CL-IR), correlation causes a strong increase in probability of failure. When only resistance is correlated (IL-CR), there is a modest falling trend. When both load and resistance are correlated (CL-CR), the effects tend to counteract each other but the effect of load correlation dominates so there is an overall increase in probability of failure.

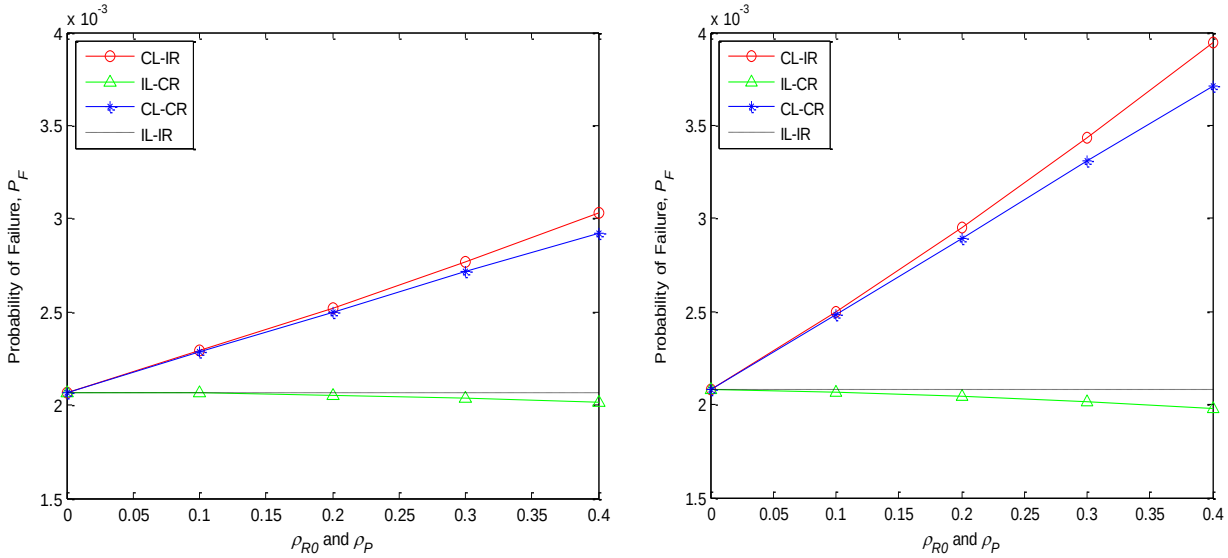

Figure 4 – Probability of failure for a range of correlation coefficients (CL = correlated load, CR = correlated resistance, IL = independent load, IR = independent resistance): (a) load sharing factor, λ = 0.5; (b) load sharing factor, λ = 1.0

For a load sharing factor of λ = 1.0, different mean resistances have been chosen, $\mu_1 = \mu_2$ =5850 (kN.m), so that the probability of failure is the same order of magnitude as before. It is found that the correlation of load and resistance has a more pronounced effect. Sensitivity of probability to correlation coefficient (slope in figure) for λ = 1.0, is about double the value of sensitivity for λ = 0.5. This is true for both rising (e.g., CL-IR) and falling (e.g., IL-CR) cases.

In further investigations it is found that the sensitivity of failure probability to correlation coefficient for loads reduces when the order of magnitude (of probability of failure) increases. To explain this issue, the bivariate normal distribution for load is shifted in a sequence of examples. Specifically, the mean values for both loads (kept equal) are varied in the range, 130-300 (kN). The standard deviation is kept constant.

The sensitivity of failure probability to correlation coefficient for loads is illustrated using Figure 5. This figure plots the failure probability per unit correlation (slope of curves in for example Figure 6) against probability of failure. As load sharing factor affects this slope, it is normalised in the figure with respect to the independent case.

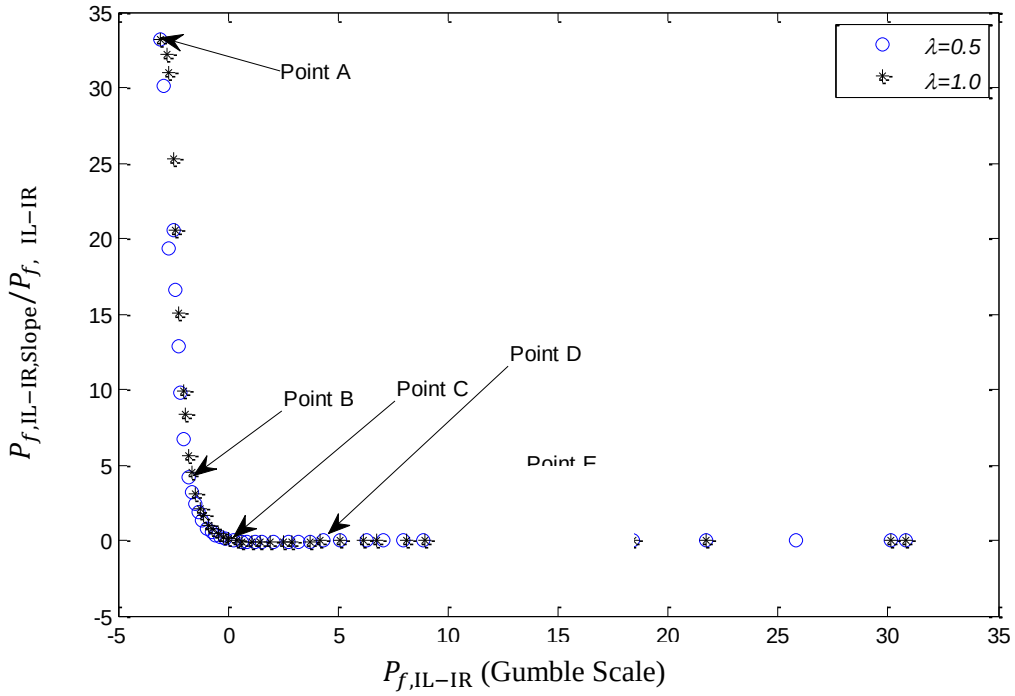

Figure 5 – Sensitivity of probability of failure, p_f, for correlated load with independent resistance case to its magnitude – varying mean value for load

It can be seen that the probability of failure is highly sensitive to correlation coefficient of load when its magnitude is small (of the order of 10^{-6}) – see Point A. This sensitivity reduces when the order of magnitude increases – see Point C etc.. Figure 6(a) through (d) show the relationships between probability of failure and correlation coefficient for different magnitudes of P_f, i.e., with one figure for each point identified in Figure 5.

For example, in Figure 6(a), the average slope, when normalised with respect to the zero correlation case (P_f=8.8×10-10), is 33.00 (Point A). For Point B on the other hand, the average slope, when normalised with P_f=2.8×10^{-3}, is 4.1.

Figure 6(d) shows negative slopes for correlated load with independent resistance which is opposite to the trend of Figure 6 (a) to Figure 6(c). However, the normalised slope shows the actual effect of correlation of P_f in this zone (i.e., 0.9-1).

4 Example 2: Multi-Point Problem with Moving Loads

A 21 m long bridge with two side-by-side beams is again considered in this example (Figure 7). The loads in the two lanes are taken from a bivariate Normal distribution with means of $\mu_1 = \mu_2 = 410$ (kN) and standard deviations of $\sigma_1 = \sigma_2 = 41$ (kN). The gap between the two loads is taken from a uniform distribution with the range (-10.5,10.5), i.e., the gap varies randomly with equal probability of any value in this range. In this study, 2.5×10^5 group of P_1, P_2 and d are simulated, where P_1 and P_2 are the

loads in lanes 1 and 2 respectively and d is the gap. Each (P_1, P_2, d) load scenario is passed over the bridge in steps of 0.5 m, to obtain the maximum load effect at each beam segment, for each event. Assuming 1.5 m long segments in each lane (14 segments in each lane; 28 in total), the maximum load effect of bending moment is calculated for all events and the maximum of 1000 bending moments for each segment is recorded as the daily maximum load effect.

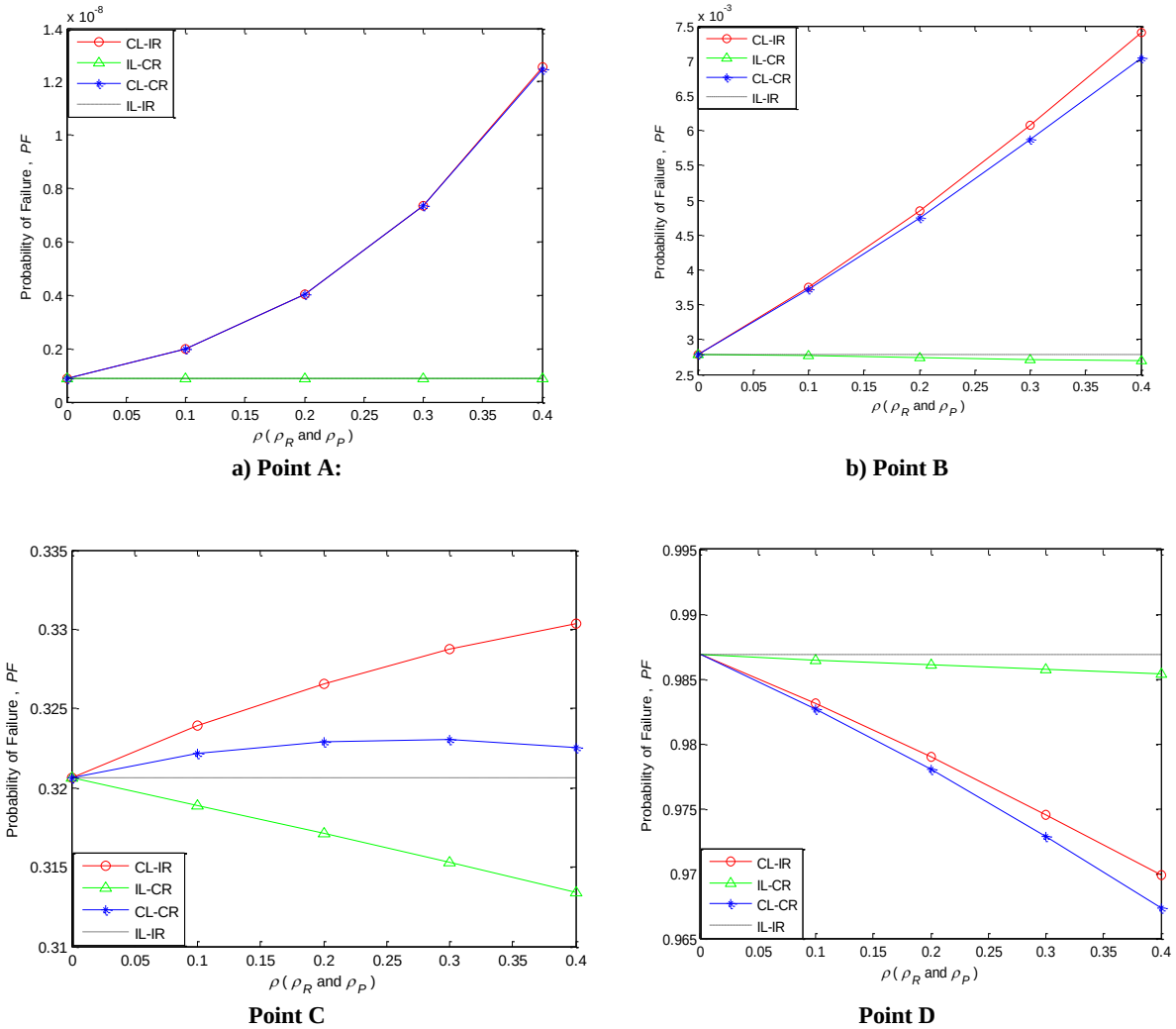

Figure 6 – Probability of failure for a range of correlation coefficients (CL = correlated load, CR = correlated resistance, IL = independent load, IR = independent resistance), load sharing factor, λ = 0.5

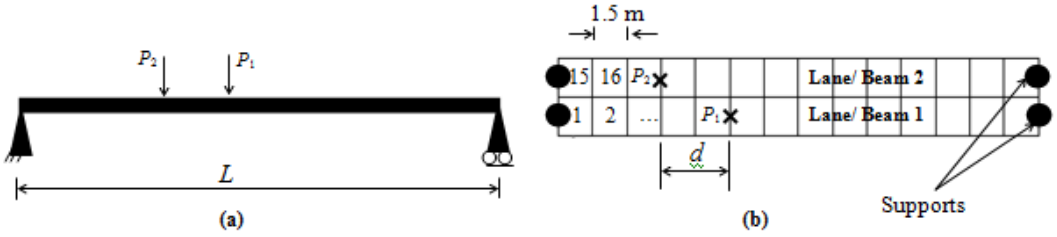

Figure 7 – Schematic of bridge with assumed segments: (a) elevation, (b) plan

The load effect in each segment of beam 1, caused by P_1, is calculated by the influence line corresponding to that segment. As before, the contribution of P_2 is calculated using the load sharing

factor concept, where in this case beam 1 is taken as the primary lane and beam 2 as the secondary one. For load effects in beam 2, this beam is taken as primary and beam 1 as secondary.

Figure 8 shows the maximum-per-day load effects on Gumbel probability paper (double log scale of cumulative distribution function (i.e., -log (-log(cdf)) for the 1st and 7th segments of lane 1, i.e., at left end and just left of centre. For each load sharing factor, the data is plotted using correlation coefficients for load ranging from 0 to 0.1 (the darker points correspond to zero correlation coefficient for load). The correlation in this range has relatively little effect but that effect is generally positive, i.e., more correlated load results in greater maximum-per-day load effect. The higher load sharing factor has a much more significant effect and causes a substantial increase in load effect. Even though the loads are not necessarily near one another, there are enough instances where they are, that the maximum-per-day load effects are 0.5% increased. For other segments, the magnitudes of the load effects are different but the general trends are similar.

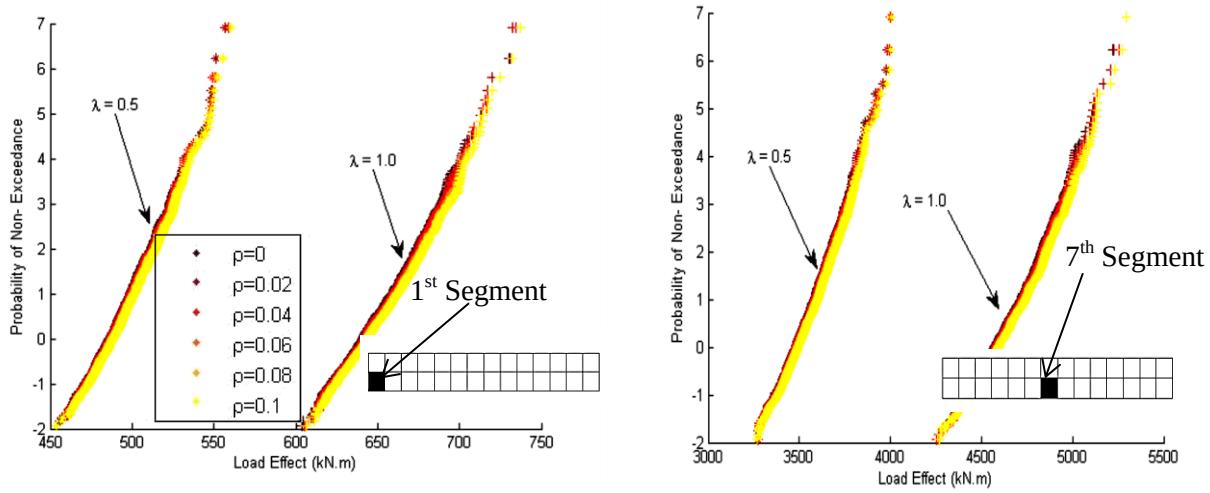

Figure 8 – Maximum-per-day load effects plotted on probability paper for two load sharing factors, λ and a range of correlation coefficients for load, ρL (greater ρL data shown in lighter colours): (a) 1st segment; (b) 7th segment

There is strong correlation between maximum-per-day load effects in adjacent segments as the maxima are likely to be caused by the same loading scenarios. This tends to diminish as the distance between the segments increases. This can be seen in the contour plots of correlation coefficient of load effect in Figure 9. For example, in the case of $\lambda = 0.5$, load effect in Segment 1 is strongly correlated with that in Segments 2 and 3. It is less strongly correlated with the segments in the 2nd lane, Nos. 15 – 28. The most likely critical loading scenario for segments, in both lanes, is the case with zero inter-lane gap (d=0).

When the load sharing factor is, λ = 1, the loading in each lane has equal weighting and the correlations are much higher (note the different legend for Figure 9(a) and (b)). In this case, Segment 1 is fully correlated with Segment 15 and is equally correlated with Segments 16 and 2, etc.. The correlation of load is found to have a modest influence on the correlation contours of load effects.

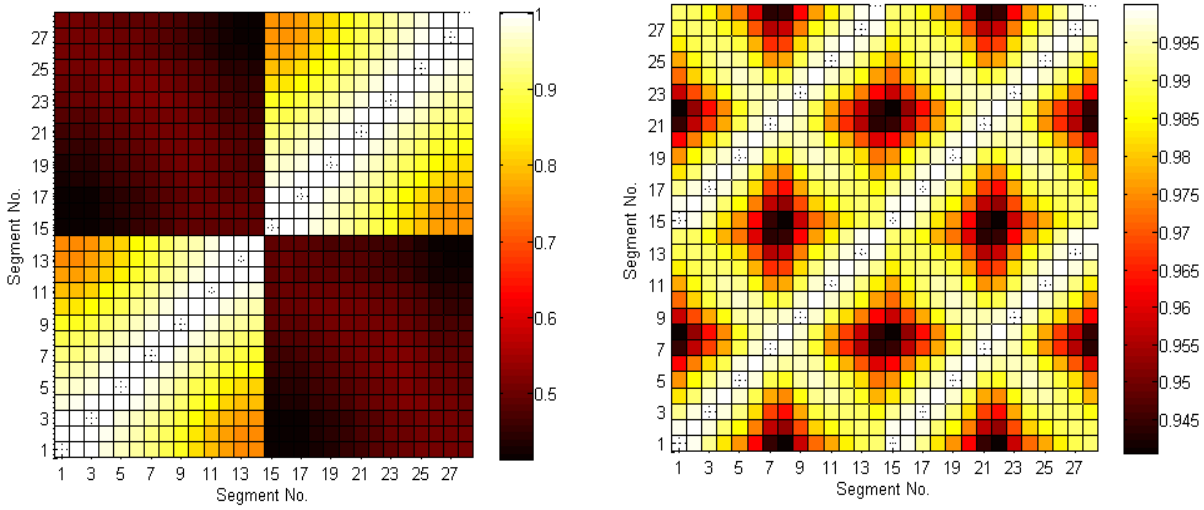

(a) λ = 0.5 **(b) λ = 1.0**

Figure 9 – Correlation coefficient between maximum-per-day load effects in segments (Nos. 1-14 refer to Lane 1 and Nos. 15-28 refer to Lane 2)

For this example, the mean resistance in the segments is the same but there is spatial variability between each segment. The resistance of each segment is taken from a Normal distribution. As explained in the previous section, different mean values are used for resistance depending on load sharing factor. For the case of $\lambda = 0.5$, the resistance is generated using a Normal distribution with mean, 5085 kN.m, and standard deviation, 400 kN.m. The mean value of resistance is chosen to be 6300 (kN.m) for $\lambda = 1.0$. Resistances for each segment are taken to be correlated according to the autocorrelation function introduced in section 1. In order to be able to investigate the effect of resistance correlation coefficient, the constant correlation term of Equation (1), ρ_{R0}, is varied within the range of 0 to 0.3; the scale of fluctuation is taken to be θ =3 m in this example.

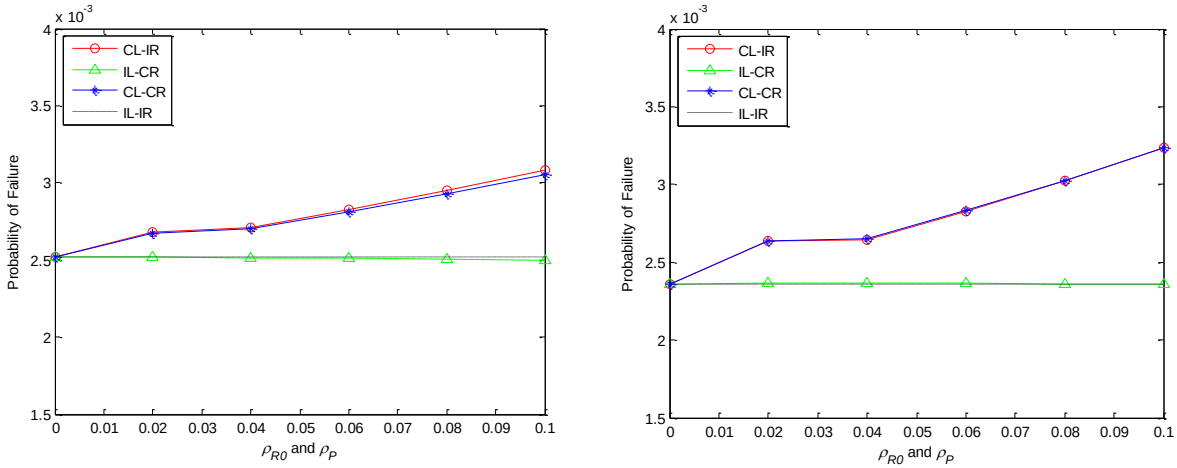

(a) **(b)**

Figure 10 – Probability of failure for range of correlation coefficient for load and resistance (CL = correlated load, CR = correlated resistance, IL = independent load, IR = independent resistance): (a) λ = 0.5, (b) λ = 1.0

Using the generated resistances and load effects for each segment, the probability of failure is calculated using MC simulation. Figure 10 presents the results for a range of correlation coefficients for load and resistance. It can be concluded that, as for the previous example, correlation of load results in a strong increase in the probability of failure whereas correlation of resistance results in a modest decrease. Figure 11 shows the influence of correlation on probability of failure in contour

plots. As for the 2-point example, the influences of load and resistance tend to counteract each other but load effect tends to dominate.

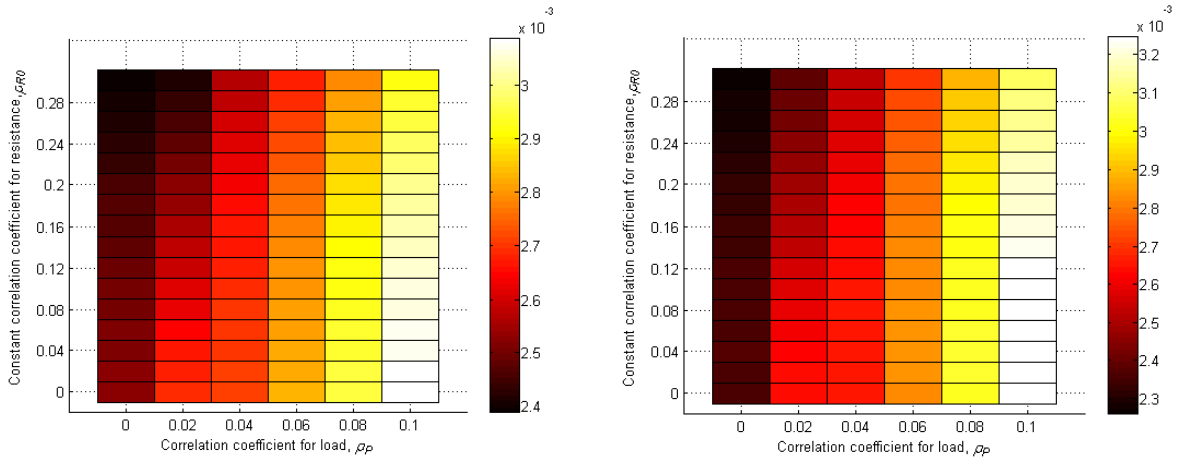

(a) **(b)**

Figure 11 – Probability of failure for range of correlation coefficients for load and resistance: (a) λ = 0.5, (b) λ = 1.0

5 Example 3: WIM-Calibrated Traffic Load Modelling on Beam-and-Slab Bridge

This section presents results from an analysis of a beam-and-slab (girder) bridge. The purpose is two-fold: (i) to eliminate the dominant effect of a simple load sharing factor for all segments and (ii) to investigate the effect of including real traffic loading scenarios from measured WIM records.

Figure 12 is a schematic illustration of a beam-and-slab (girder) bridge deck consisting of a cast in-situ slab on precast concrete Y3-beams/girders (Taylor et al. 1990). Each precast beam is supported on a bearing at each end, the deck has a single span of 21 m (centre to centre of bearings), and is 9 m wide. The elastic modulus of the precast beams and in-situ slab is 30×10^3 N/mm^2. In the finite element analyses, the slab is modelled using rectangular plate elements with both bending and membrane capabilities, i.e., six degrees of freedom per node. The beam and plate elements are assumed be in the same plane. The properties of the longitudinal beam members are determined from the properties of the actual beams and the portion of slab above them. The section properties for the beam-and-slab deck are generally calculated about the centroid of the composite section (OBrien and Keogh 1999).

For a slab depth of 0.15 m, Figure 13 illustrates the bending moment due to a single unit axle load (shown in Figure 12) at $X_P = 0.5$ m and $X_P = 10.5$ m from the left end of the first lane (P_1) (shaded area in Figure 12), for Girders 1 and 2 (X_S represents the segment's longitudinal position). For load in lane 1, the bending moment diagram for load at mid-span is quite 'rounded' for Girder 1 (Figure 13(a)) due to load sharing. It is more 'peaked' for Girder 2 with load in lane 1 as the girder is directly beneath one of the axle loads. For load in lane 2, the moment is much less and the diagrams are far more rounded.

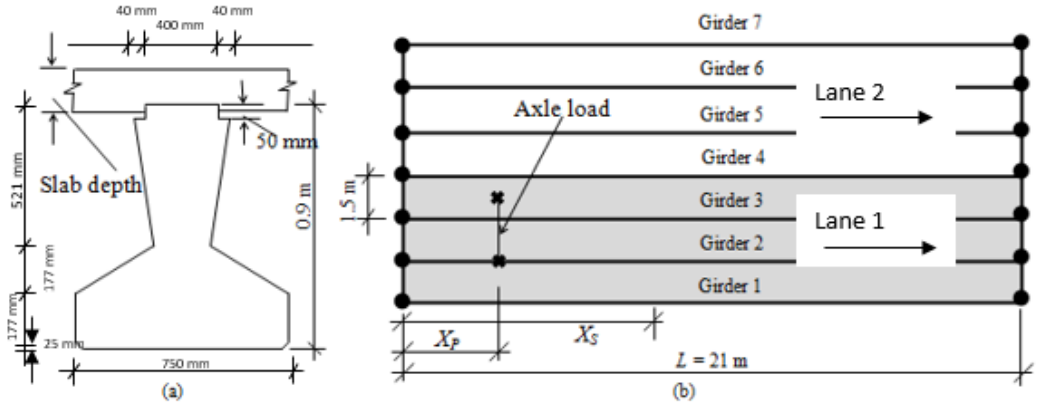

Figure 12 – Schematic of Beam-and-Slab Bridge: (a) Y-beam Cross Section (dimensions in mm), (b) Plan view

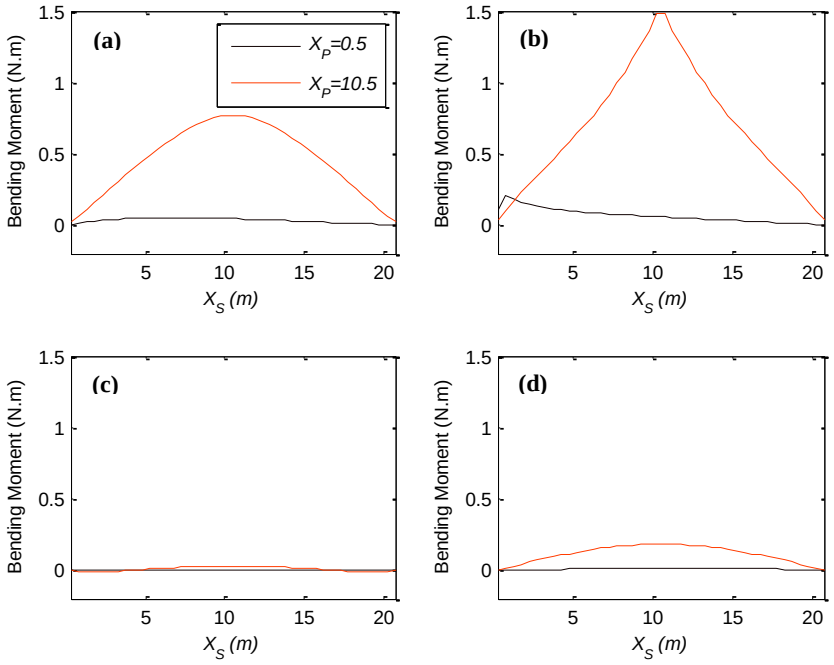

Figure 13 – Bending moment due to unit axle load: (a) Girder 1, load in lane 1; (b) Girder 2, load in lane 1; (c) Girder 1, load in lane 2; (d) Girder 2, load in lane 2

The ratio of moment in the girders due to load in lane 2, to the corresponding moment due to load in lane 1, is shown in Figure 14. This ratio can be viewed as a segment-specific load sharing factor. It can be seen to vary significantly with segment (i.e., with X_S) and in some cases (Figure 14(b)), varies also with load location.

Figure 15 illustrates the load sharing factors corresponding to when the slab thickness has doubled to 0.3 m. While this is an extreme case, it serves to illustrate the increased load sharing (greater load sharing factors) when the bridge is stiffer transversely.

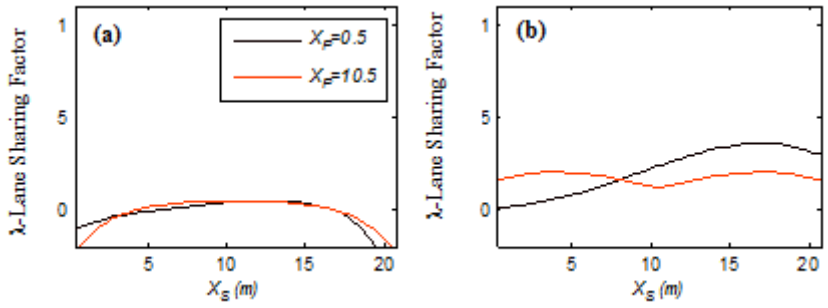

Figure 14 – Segment-specific load sharing factor for load at X_P=0.5 and X_P=10.5: (a) Girder 1; (b) Girder 2

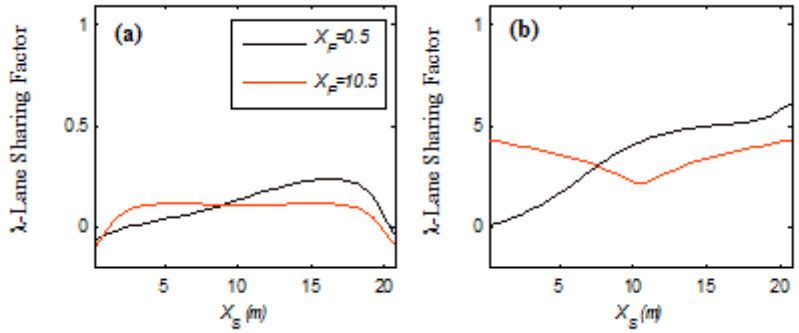

Figure 15 – Segment-specific load sharing factor for load at XP=0.5 and XP=10.5 for greater slab thickness: (a) Girder 1; (b) Girder 2

A simple probabilistic load model is used, in this example similar to the HL-93 model (AASHTO 2007). It consists of a uniformly distributed loading and a 3-axle vehicle (Figure 16) in each lane. However, in this case, the load model is probabilistic: the intensity of the uniform loading and the gross weight of the vehicles are Weibull distributed. The distribution parameters, given in Table 1, are chosen by trial and error to give cumulative probabilities that approximately match those found by Leahy (2014). Leahy's distributions are calibrated against WIM data recorded at a heavily trafficked site in the Netherlands so that, while this is just an example, the results should be realistic.

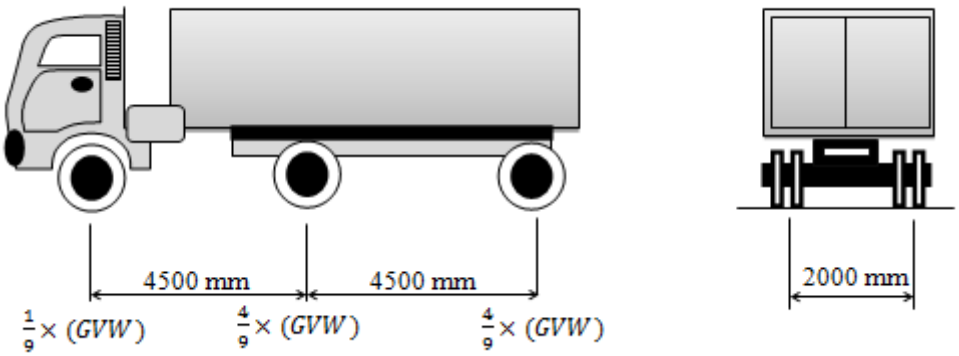

Figure 16 – Schematic drawing of truck load model

Table 1 – GEV parameters for traffic load model

	μ	σ	ξ
Load in Slow Lane (GVW_1) (kN)	620	75	-0.4
Load in Fast Lane (GVW_2) (kN)	300	75	-0.1
Uniformly distributed load (kN/m)	9	1.5	0.0

Figure 17 illustrates the distributions that result from the notional traffic load model and WIM data on the 20 m bridge on a Gumbel scale plot (i.e., double log of cumulative distribution function). In this figure, S1-HL93 is the mid-span bending moment calculated in the slow lane due to the notional truck model, given the parameters in Table 1, and S1-WIM is the bending moment due to actual traffic using WIM data. S2-HL93 and S2-WIM are distributions due to notional HL93 and WIM data in the fast lane respectively. It can be seen from the figure that the parameters used for both lanes are giving a very good match (i.e., less than 1 mean squared error) to those found from WIM data. The optimised parameters are given in Table1.

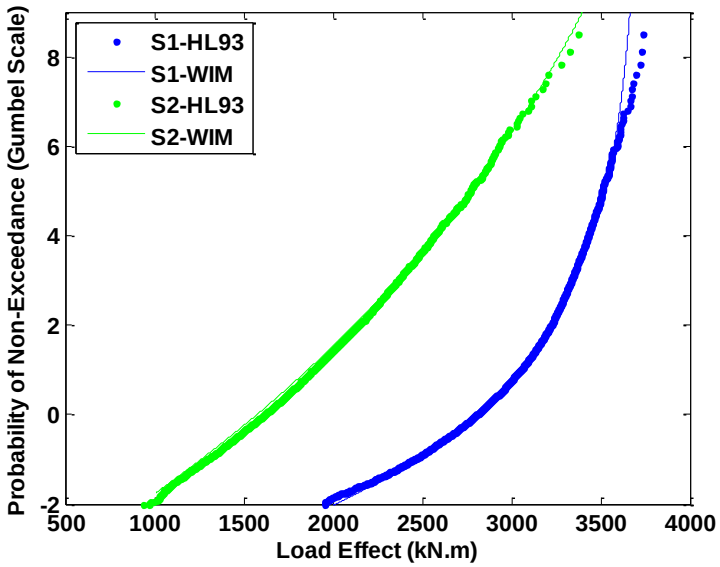

Figure 17 – Mid-span bending moments for notional load model and measured WIM data

Assuming 1.5 m long segments, the resistance at each segment is generated using the normal distribution with mean of 2040 (kN.m) and standard deviation of 400 (kN.m). Resistance values are taken to be correlated using the autocorrelation function given in Equation (1) with assumed values, $\theta_x = \theta_y = 3$. As in the previous example, the constant correlation term in Equation (1) is varied in the range of 0 to 0.3, to investigate the effect of increasing resistance correlation coefficient.

Probability of failure is estimated for each combination of correlation coefficient in the range considered. Figure 18 shows that, by eliminating the effect of constant load sharing factor for all segments and all load positions, the sensitivity to load correlation coefficient is greatly reduced. As explained in the first simple example, load effect correlation is more affected by load sharing factor than by correlation of load. In this example, a different load sharing factor is applied for each element and each load position based on the 'true' (finite element-calculated) transverse load sharing through the slab. It is clear that load effect is much less correlated than is implied by assuming a constant load sharing factor. The minimum load sharing factor used in the first two examples was 0.5, whereas, in this example, the load sharing factor varies within a range of -0.4 to 0.05 for the first girder, 0 to 0.4

for the second and 0 to 0.8 for Girder 3. As a result of the reduced load sharing factors, load effects are much less correlated than in the first two examples. Consequently, the sensitivity of probability of failure to load correlation is significantly reduced (i.e., less than 0.01% increase in probability of failure) in this example in comparison to previous examples.

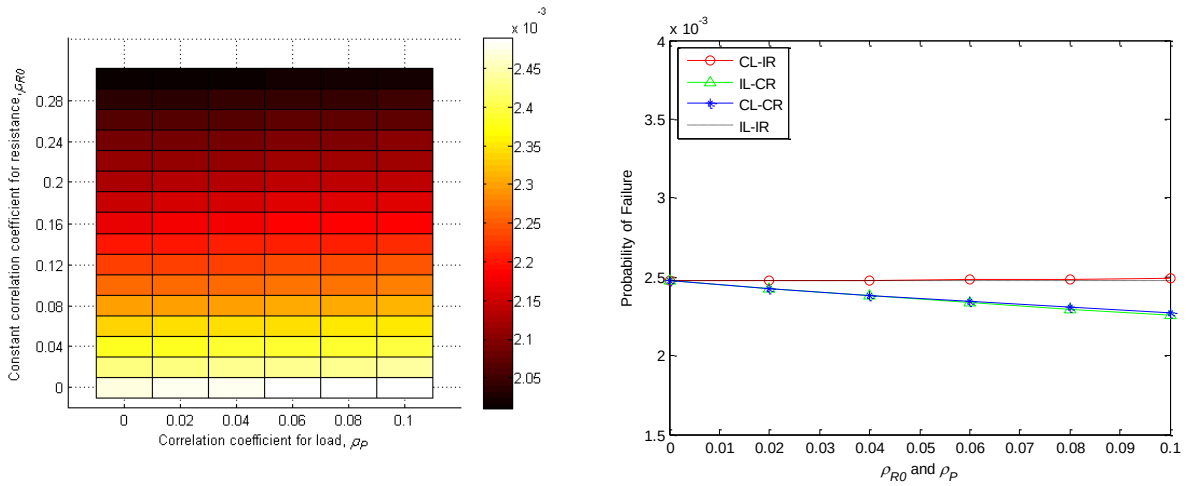

(a) **(b)**

Figure 18 – Probability of failure for a range of correlation coefficients for load and resistance for beam-and-slab bridge (CL = correlated load, CR = correlated resistance, IL = independent load, IR = independent resistance): (a) Contour plot; (b) Section through

6 Conclusions

Three examples are considered in this investigation of load and resistance spatial correlations and its effect on probability of failure. In the first, just two loads are considered that are fixed at the centre of the bridge. An exaggerated level of load correlation shows that it can significantly (i.e., increased by 40%) affect the calculated probability of failure. Even for weak levels of load correlation, load effect is shown to be strongly correlated and allowing for this has an even more significant influence on the calculated probability of failure. Allowing for correlation of resistance reduces the failure probability, but only moderately.

A second example considers a bridge made up of just two beams but, in this case, the loads can travel along the beam and the gap between them is allowed to vary stochastically. In this case, each beam is divided into segments and failure is defined as when the load effect at any one of the segments exceeds its resistance. Correlation of load effect and resistance is allowed between all segments in both beams. In this example a more sophisticated pattern of load effect correlation is apparent and a spatially-dependent resistance correlation function is introduced. The end result is similar to the first example: allowing for correlation of load effect has a significant (i.e., increased by 20%) influence on probability of failure. Correlation of resistance is less influential and has an opposing effect on probability of failure.

The third example is a more realistic beam-and-slab bridge. It replaces the simple load sharing factors used in the other examples with realistic factors derived for each segment in each girder for each load location based on a finite element analysis. The same trends as before are apparent but, when accurate load sharing factors are used for all girders, the sensitivity of failure probability to correlation is greatly reduced.

It can be concluded from the results that the probability of failure depends on both load and resistance correlation but the effect is generally small. The effect of correlation on probability of failure is found to be also a function of the order of magnitude of probability..

7 Acknowledgement

This work is supported under the TEAM project. TEAM is a Marie Curie Initial Training Network and is funded by the European Commission 7th Framework Programme (PITN-GA-209-238648).

References

Akgül, F. and Frangopol, D. M. (2004). Time-Dependent Interaction between Load Rating and Reliability of Deteriorating Bridges. Engineering Structures, 26(12), 1751-1765.

Akiyama, M., Frangopol, D. M. and Yoshida, I. (2010). Time-Dependent Reliability Analysis of Existing Reinforced Concrete Structures in a Marine Environment Using Hazard Associated with Airborne Chlorides. Engineering Structures, 32(11), 3768-3779.

Ang, A. H. S. and De Leon, D. (2005). Modeling and Analysis of Uncertainties for Risk-Informed Decisions in Infrastructures Engineering. Structure and Infrastructure Engineering: Maintenance, Management, Life-Cycle Design and Performance, 1(1), 19-31.

Ang, A. H. S. and Tang, W. H. (2007). Probability Concepts in Engineering Planning and Design - Basic Principles. Unites States of America, John Wiley & Sons Inc.

Castillo, E., Hadi, A. S., Balakrishnan, N. and Sarabia, J.-M. (2005). Extreme Value and Related Models with Applications in Engineering and Science. Unites States of America, John Wiley & Sons Inc.

Darmawan, M. S. and Stewart, M. G. (2007). Spatial Time-Dependent Reliability Analysis of Corroding Pretensioned Prestressed Concrete Bridge Girders. Structural Safety, 29(1), 16-31.

Der Kiureghian, A. and Ke, J.-B. (1988). The Stochastic Finite Element Method in Structural Reliability. Probabilistic Engineering Mechanics, 3(2), 83-91.

Ellingwood, B. R. (2005). Risk-Informed Condition Assessment of Cvil Infrastructure: State of Practice and Research Issues. Structure and Infrastructure Engineering, 1(1), 7-18.

Engelund, S. and Sørensen, J. D. (1998). A Probabilistic Model for Chloride-Ingress and Initiation of Corrosion in Reinforced Concrete Structures. Structural Safety, 20(1), 69-89.

Enright, B. (2010). Simulation of Traffic Loading on Highway Bridges. PhD Thesis, University College Dublin, Dublin, Ireland.

Enright, M. P. and Frangopol, D. M. (1999). Reliability-based Condition Assessment of Deteriorating Concrete Bridges Considering Load Redistribution. Structural Safety, 21(2), 159-195.

Frangopol, D. M. (2011). Life-cycle performance, management, and optimisation of structural systems under uncertainty: accomplishments and challenges. Structure and Infrastructure Engineering, 7(6), 389-413.

Gindy, M. and Nassif, H. H. (2007). Multiple Presence Statistics for Bridge Live Load Based on Weigh-in-Motion Data. Transportation Research Record: Journal of the Transportation Research Board, 2028(1), 125-135.

Haldar, A. and Mahadevan, S. (2000). Reliability Assessment Using Stochastic Finite Element Analysis. Unites States of America, John Wiley & Sons Inc.

Karimi, A. (2002). Probabilistic assessment of Deterioration and Strength of Concrete Bridge Beams and Slabs. PhD Thesis, Imperial College of Science, Technology and Medicine, London, United Kingdom.

Karimi, A., Ramachandran, K., Buenfeld, N. and Crowder, M. (2005). Probabilistic Analysis of Reinforcement Corrosion with Spatial Variability. Ninth International Conference on Structural Safety and Reliability, ICOSSAR 05, Rotterdam, Netherlands.

Kenshel, O. and O'Connor, A. J. (2009). Assessing Chloride-Induced Deterioration in Condition and Safety of Concrete Structures in Marine Environments. European Journal of Environmental and Civil Engineering, 13(5), 593-613.

Kersner, Z., Novák, D., Teply, B. and Rusina, R. (1998). Modeling of Deterioration of Concrete Structures by Stochastic Finite Element Method. Seventhth Intenational Conference on Structural Safety and Reliability, ICOSSAR 97, Kyoto, Japan, A. A. Balkema.

Kulicki, J. M., Prucz, Z., Clancy, C. M., Mertz, D. R. and Nowak, A. S. (2007). Updating the Calibration Report for AASHTO-LRFD code. Final Report for National Cooperative Highway Research Program (NCHRP). Washington DC, United States of America, Transportation Research Board.

Leahy, C. (2014). Using Weigh-in-Motion Data to predict extreme Traffic loading on Bridges. PhD Thesis, University College Dublin, Dublin, Ireland.

Li, C.-C. and Der Kiureghian, A. (1993). Optimal Discretization of Random Fields. Journal of Engineering Mechanics, 119(6), 1136-1154.

Li, Y. (2004). Effect of Spatial Variability on Maintenance and Repair Decisions for Concrete Structures. PhD Thesis, TU Delpth, Delfth University of Technology, Delfth, Netherlands.

Li, Y., Vrouwenvelder, T., Wijnants, G. and Walraven, J. (2004). Spatial Variability of Concrete Deterioration and Repair Strategies. Structural Concrete, 5(3), 121-129.

Malioka, V. and Faber, M. H. (2004). Modeling of the Spatial Variability for Concrete Structures. Bridge Maintenance, Safety, Management and Cost - IABMAS 04, Rotterdam, Netherland, A. A. Balkema.

Marsh, P. S. and Frangopol, D. M. (2008). Reinforced Concrete Bridge Deck Reliability Model Incorporating Temporal and Spatial Variations of Probabilistic Corrosion Rate Sensor Data. Reliability Engineering & System Safety, 93(3), 394-409.

Melchers, R. E. (1999). Structural Reliability: Analysis and Prediction. Unites States of America, John Wiley & Sons Inc.

Mori, Y. and Ellingwood, B. R. (1993). Reliability-based Service-Life Assessment of Aging Concrete Structures. Journal of Structural Engineering, 119(5), 1600-1621.

Nowak, A. S. (1993). Live Load Model for Highway Bridges. Structural Safety, 13(1-2), 53-66.

O'Connor, A. J. and Kenshel, O. (2012). Experimental Evaluation of the Scale of Fluctuation for Spatial Variability Modeling of Chloride-Induced Reinforced Concrete Corrosion. Journal of Bridge Engineering, 18(1), 3-14.

OBrien, E. J. and Enright, B. (2011). Modeling Same-Direction Two-Lane Traffic for Bridge Loading. Structural Safety, 33(4-5), 296-304.

OBrien, E. J. and Keogh, D. L. (1999). Bridge deck analysis. United Kingdom, United States of America and Canada, Taylor & Francis Group.

Papadrakakis, M. and Lagaros, N. D. (2002). Reliability-based structural optimization using neural networks and Monte Carlo simulation. Computer Methods in Applied Mechanics and Engineering, 191(32), 3491-3507.

Sivakumar, B., Ghosn, M. and Moses, F. (2011). Protocols for collecting and using traffic data in bridge design. Report of National Cooperative Highway Research Program. Washington DC, United States of America, Transportation Research Board.

Sivakumar, B., Moses, F., Fu, G. and Ghosn, M. (2007). Legal truck loads and AASHTO legal loads for posting. Transportation Research Board National Research.

Sterritt, G., Chryssanthopoulos, M. K. and Shetty, N. (2001). Reliability-based Inspection Planning for RC Highway Bridges. Safety, Risk and Reliability-Trends in Engineering, Zurich, Switzerland, International Association for Bridge and Structural Engineering.

Stewart, M. G. (2004). Spatial Variability of Pitting Corrosion and its Influence on Structural Fragility and Reliability of RC Beams in Flexure. Structural Safety, 26(4), 453-470.

Stewart, M. G. (2005). Life-Cycle Cost analysis Considering Spatial and Temporal Variability of Corrosion-Induced Damage and Repair to Concrete Surface. International Conference on Structural Safety and Reliability, ICOSSAR 05.

Stewart, M. G. (2006). Spatial Variability of Damage and Expected Maintenance Costs for Deteriorating RC Structures. Structure & Infrastructure Engineering, 2(2), 79-90.

Stewart, M. G. (2009). Mechanical Behaviour of Pitting Corrosion of Flexural and Shear Reinforcement and its Effect on Structural Reliability of Corroding RC Beams. Structural Safety, 31(1), 19-30.

Stewart, M. G. and Al-Harthy, A. (2008). Pitting Corrosion and Structural Reliability of Corroding RC Structures: Experimental Data and Probabilistic Analysis. Reliability Engineering & System Safety, 93(3), 373-382.

Stewart, M. G., Estes, A. C. and Frangopol, D. M. (2004). Bridge deck replacement for minimum expected cost under multiple reliability constraints. Journal of Structural Engineering, 130(9), 1414-1419.

Stewart, M. G. and Mullard, J. A. (2007). Spatial Time-Dependent Reliability Analysis of Corrosion Damage and the Timing of First Repair for RC Structures. Engineering Structures, 29(7), 1457-1464.

Stewart, M. G. and Rosowsky, D. V. (1998). Time-dependent reliability of deteriorating reinforced concrete bridge decks. Structural Safety, 20(1), 91-109.

Stewart, M. G., Rosowsky, D. V. and Val, D. V. (2001). Reliability-based bridge assessment using risk-ranking decision analysis. Structural Safety, 23(4), 397-405.

Stewart, M. G. and Suo, Q. (2009). Extent of Spatially Variable Corrosion Damage as an Indicator of Strength and Time-Dependent Reliability of RC Beams. Engineering Structures, 31(1), 198-207.

Sudret, B., Defaux, G. and Pendola, M. (2007). Stochastic Evaluation of the Damage Length in RC Beams Submitted to Corrosion of Reinforcing Steel. Civil Engineering and Environmental Systems, 24(2), 165-178.

Taylor, H. P. J., Clark, L. A. and Banks, C. C. (1990). The Y-beam: a replacement for the M-beam in beam and slab bridge decks. The Structural Engineer, 68(23), 459-465.

Val, D. V., Stewart, M. G. and Melchers, R. E. (2000). Life-Cycle Performance of RC Bridges: Probabilistic Approach. Computer-Aided Civil and Infrastructure Engineering, 15(1), 14-25.

Vanmarcke, E. (1985). Random Fields: Analysis and Synthesis. London, United Kingdom, MIT Press.

Vu, K., Stewart, M. G. and Mullard, J. (2005). Corrosion-induced cracking: experimental data and predictive models. ACI Structural Journal, 102(5), 719-726.

Vu, K. A. and Stewart, M. G. (2005). Predicting the Likelihood and Extent of Reinforced Concrete Corrosion-Induced Cracking. Journal of Structural Engineering, 131(11), 1681-1689.

Vu, K. A. T. (2003). Corrosion-Induced Cracking and Spatial Time-Dependant Reliability Analysis of Reinforced Concrete Structures. PhD Thesis, The University of Newcastle, Newcastle, Australia.

Vu, K. A. T. and Stewart, M. G. (2000). Structural Reliability of Concrete Bridges Including Improved Chloride-Induced Corrosion Models. Structural Safety, 22(4), 313-333.

Zhai, X. and Stewart, M. G. (2010). Structural Reliability Analysis of Reinforced Grouted Concrete Block Masonry Walls in Compression. Engineering Structures, 32(1), 106-114.